Hindawi
Structural Control and Health Monitoring
Volume 2023, Article ID 6968338, 16 pages
https://doi.org/10.1155/2023/6968338

Research Article

Theoretical and Experimental Study on Homologous Acoustic Emission Signal Recognition Based on Synchrosqueezed Wavelet Transform Coherence

Jingkai Wang,[1] **Linsheng Huo**,[1] **Chunguang Liu**,[1] **and Gangbing Song**[2]

[1]*State Key Laboratory of Coastal and Offshore Engineering, Dalian University of Technology, Dalian 116024, China*
[2]*Smart Materials and Structures Laboratory, Department of Mechanical Engineering, University of Houston, Houston, TX 77204, USA*

Correspondence should be addressed to Linsheng Huo; lshuo@dlut.edu.cn

Received 26 September 2022; Revised 13 July 2023; Accepted 26 July 2023; Published 21 August 2023

Academic Editor: Jun Li

Copyright © 2023 Jingkai Wang et al. This is an open access article distributed under the Creative Commons Attribution License, which permits unrestricted use, distribution, and reproduction in any medium, provided the original work is properly cited.

The acoustic emission (AE) technique has been widely investigated for its ability to locate damage in structures. However, the selection of the arrival point of AE signals and the existence of nonhomologous AE signals can significantly affect the location accuracy of damages. The synchrosqueezed wavelet transform (SWT) was used in our previous research to pick the accurate arrival point, but the existence of the nonhomologous signals was neglected in the picking process. To address this limitation, the synchrosqueezed wavelet transform coherence (SWTC) method is proposed to improve the accuracy by recognizing homologous signals and suppressing the spectral leakage in this paper. Compared with the wavelet transform coherence (WTC) method previously used, the SWTC method using the squeezing wavelet coefficients obtained by the SWT can constitute a more explicit coherence graph of AE signals. This clear coherence graph can help reduce the effect of subjective factors in observing the coherence and improve the recognition accuracy of homologous signals. The effectiveness of the proposed method is experimentally verified on a steel pipe and a concrete beam. The results demonstrate that the SWTC accurately identifies homologous AE signals and effectively improves the localization accuracy across different signal densities, localization distances, and materials.

1. Introduction

Structural health monitoring (SHM) has been advancing rapidly in recent years to address the impacts of common adverse factors, such as corrosion [1], vibration and fatigue [2], and excessive loads [3], on structures across different engineering fields. Various SHM methods, including vision-based [4], ultrasonic wave-based [5], modal-based [6], and vibration-based [7] methods, have been developed with the goal of rapidly and accurately detecting damage. Among these nondestructive testing approaches, the acoustic emission (AE) technique [8, 9], which is a passive monitoring technique that measures the elastic wave released by deformation or fracture of the materials under stress [10], is more sensitive to damage and suitable for continuous health monitoring in real time [11]. These advantages make the AE technique widely applied in mechanical engineering [12, 13], civil engineering [14, 15], mining engineering [16], and other fields [17, 18]. Since the AE signals are generated when the materials become damaged, the AE signals can not only contain much information about the damage but can also be used to locate the damage [19, 20]. However, the AE-based localization method faces challenges in accurately picking the arrival point of AE signals and recognizing the homologous AE signals. Our previous research [21] proposed the synchrosqueezed wavelet transform (SWT) to accurately pick the arrival point, but the recognition of homologous AE signals is a yet unsolved problem. The homologous AE signals are emitted by the same source of damage. Therefore, by analyzing the homologous signals collected by AE sensors, it is possible to accurately determine the location of the damage source. However, the collected AE signals usually

contain the homologous and nonhomologous signals. These nonhomologous signals influence the localization accuracy by interfering with the time difference of arrival (TDOA) of signals [22]. Hence, the accurate identification of the homologous signals is beneficial to improve localization accuracy.

Many methods have been proposed for identifying homologous signals in the AE, speech, and volcanic tremor. Chen et al. [22] proposed the assumption that homologous signals should have similar characteristics (such as waveform), and they used concrete thermal-cracking experiments to demonstrate the validity of the assumption. Multiple algorithms, such as Pearson's correlation coefficient [23], the longest common subsequence algorithm [24], and edit distance on the real sequence [25], are available for investigating the similarity of a time series. Among such algorithms, dynamic time wrapping (DTW) [26, 27], which finds the minimum space distance between two time series by providing nonlinear alignments based on the standard of dynamic time warping [28], is one of the most popular algorithms used to calculate the Euclidean distance (ED) between time series. The ED between two time series is commonly used to evaluate their similarity degree, with smaller ED denoting higher similarity [29, 30]. The wrapping process allows the DTW to evaluate the similarity of nonequal-length time series [31]. Sakoe and Chiba [32] leveraged this wrapping process to identify continuous speech. Sharma et al. [33] proposed a new road surface monitoring system based on the DTW to identify road irregularities. Besides the ED, the area between time series is also an often-used metric to evaluate similarity. The normalized cross-correlation (NCC) [34], which calculates the inner product between two different signals, is a widely used area-based similarity recognition algorithm [35]. It has been widely used in electrocardiogram (ECG) signal processing [36], audio/speech signal processing [37–39], and big data analysis [40]. Klausen and Robbersmyr [41] applied the NCC to calculate the cross-correlation between a whitened vibration signal and its envelope to analyze bearing faults. Nguyen et al. [42] used the cross-correlation image to identify the defects in pipelines. The convolution operation in the NCC helps determine the time-based shift between two signals [40], which can be used to calculate the time delay of signals used for localization [43, 44]. Permana et al. [45] used the characteristic of the NCC to locate a volcanic tremor source. However, the convolution causes the NCC to become overly sensitive towards minor distortions in the time axis [46] and also causes the recognition accuracy to become vulnerable to noise and frequency dispersion.

However, the above similarity recognition algorithms are operated in the time domain, which precludes their usage in the time-frequency domain. In general, time-frequency analysis more comprehensively reflects the intrinsic characteristics of signals than with time domain analysis [47]. Therefore, the time-frequency analysis has played a crucial role in SHM [48], and many time-frequency analysis algorithms, including fast Fourier transform (FFT), wavelet transform (WT), and Hilbert–Huang transform (HHT), have served as the foundation for developing methods to analyze damage signals. Katunin and Sun et al. combined the vibration-based method and wavelet transform (WT) to detect the damage of sandwich composites [49, 50]. Chakraborty et al. utilized wavelet transform to identify the corresponding mode shapes from the transient response of the system under ambient vibration conditions [51] and proposed an online time-varying stiffness monitoring system [52]. Furthermore, they combined time-frequency-based signal processing methods with clustering algorithms to efficiently identify modal parameters [53]. For analyzing the similarity in the time-frequency domain, Torrence and Compo [54] proposed the wavelet transform coherence (WTC), which is a time-frequency similarity recognition algorithm. This algorithm converts the time domain signals to time-frequency matrices through wavelet transform and evaluates the similarity by calculating the coherence between time-frequency matrices. As a result, the coherence graph shows the similarity between signals in the time and frequency axes. Gao et al. [55] applied the WTC and AE analysis to study the relationship between the pure metal burn signals and grinding burn signals. Grinsted et al. [56] applied WTC to study the Arctic Oscillation index and the Baltic maximum sea ice extent record. Kramer et al. [57] used the WTC to distinguish tremor types between organic and functional types effectively.

Despite a large volume of research for WTC, there are still some crucial problems yet to be solved. First, the point-to-point coherency process [58] shows that the WTC is very sensitive to the energy distribution change in the time-frequency domain. Therefore, precise and clear energy distribution in the time-frequency domain is crucial for accurate coherency analysis. However, the spectrum leakage using continuous wavelet transform (CWT) causes the distribution of instantaneous amplitudes in the time-frequency matrix to be blurred [59], suggesting that the WTC based on the CWT cannot accurately reflect the similarity between AE signals. Second, the accuracy in recognizing homologous signals through the coherence graph is susceptible to subjective factors, and thus, an objective quantitative coefficient for analyzing a coherence graph is necessary. Finally, it will take much computing time to sequentially obtain the coherence graphs of every two signals in a larger amount of data. The defects mentioned previously can cause the low recognition accuracy of existing methods of recognizing homologous signals.

In this paper, the synchrosqueezed wavelet transform coherence (SWTC) recognition method is proposed to improve the recognition accuracy of homologous AE signals. The proposed method uses the SWT to replace the CWT, thereby improving the clarity degree of coherence graphs by suppressing the spectrum leakage. Meanwhile, the SWTC coefficient is used to gauge the similarity degree of the coherence graph, reducing the influence of subjective factors in observing the coherence graph. In addition, the proposed method also improves computational efficiency by combining the time-order approach. The pencil lead fracture (PLF) experiments on a steel pipe and a concrete beam were conducted to verify the effectiveness of the proposed method.

2. Synchrosqueezed Wavelet Transform Coherence-Based Recognition of Homologous AE Signals

2.1. Flowchart of the Novel Method. This paper proposes the SWTC method to improve the accuracy in recognizing homologous signals, and a detailed flowchart of this method is presented in Figure 1. The collected AE signals are first divided into different localization groups by the time-order method, which can preliminarily identify the homologous signals by the arrival time of AE signals. Each localization group is composed of the localization pair and velocity measurement pair. The localization pair is used to locate the damage source, and the velocity measurement pair at a known distance is used to determine the wave velocity of AE signals. Then, the SWTC coefficients of these pairs are computed to reflect the similarity degree of AE signals. When the SWTC coefficients of the localization pair and velocity measurement pair in the localization groups are higher than the mean value of all SWTC coefficients, the localization groups are used to compute the accurate localization values. The detailed process is described in the following section.

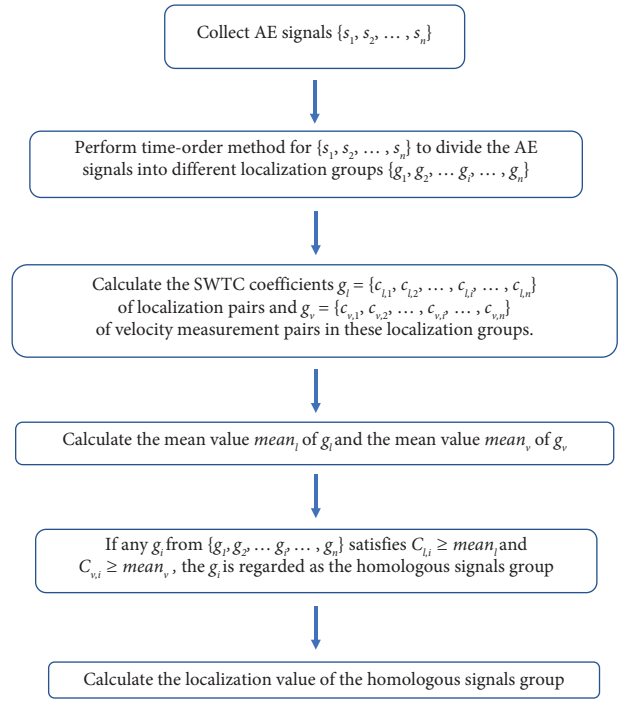

Figure 1: The flowchart of the SWTC recognition method.

2.2. Detailed Process of the Novel Method. A large amount of AE signals can be collected in an experiment (as shown in Figure 2). The traditional similarity recognition methods, which sequentially compute the coherence value between the selected signals and other signals, require much computing time. To solve this problem, the time-order method [21] is used to filter out the interference signals and divide the potential homologous AE signals into different localization groups ($\{g_1, g_2, \cdots, g_n\}$) with less computation time. However, the localization groups are composed of the homologous AE signals and the nonhomologous AE signals, and thus the localization groups need to be further filtered.

For a random localization group g_i from $\{g_1, g_2, \cdots, g_n\}$, it contains four AE signals $\{x_1, x_2, x_3, x_4\}$. The AE signals $\{x_2, x_3\}$ collected from sensors s_2 and s_3 (as shown in Figure 2) are the localization pair p_l, and the AE signals $\{x_1, x_2\}$ (or $\{x_3, x_4\}$) collected from sensors s_1 and s_2 (or s_3 and s_4) are the velocity measurement pair p_v. For the AE signal x_1 from the velocity measurement pair p_v, the wavelet coefficient can be expressed as follows:

$$W_1(a,b) = \langle x_1, \psi_{a,b} \rangle = \int_{-\infty}^{\infty} x_1(t) \frac{1}{a} \overline{\psi\left(\frac{t-b}{a}\right)} dt, \quad (1)$$

where a is the scale variable, which controls the dilation of the mother wavelet function $\psi_{a,b}$, and b is the time variable, which controls the translation of the mother wavelet function [60]. Considering that the analyzed signals are AE signals, the complex Morlet wavelet is chosen as the wavelet basis [61]. According to reference [62], the candidate's instantaneous frequency $\omega_1(a,b)$ of the AE signal x_1 is described as follows:

$$\omega_1(a,b) = \frac{\partial W_1(a,b)/\partial b}{2\pi i W_1(a,b)}. \quad (2)$$

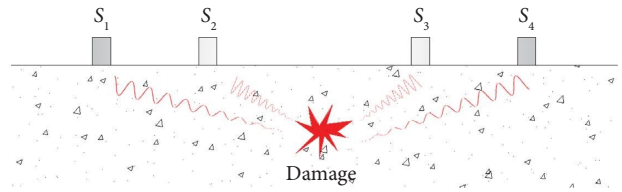

Figure 2: The distribution of AE sensors in the time-order filtering algorithm.

The wavelet coefficients (the red circle in Figure 3) with frequency for which the distance away from $\omega_1(a,b)$ is ξ in the frequency domain will be squeezed and reassigned around the candidate's instantaneous frequency $\omega_1(a,b)$:

$$T_1(\xi,b) = \int_{\{a:W_1(a,b)\neq 0\}} W_1(a,b)\delta(\omega_1(a,b) - \xi)\frac{da}{a}, \quad (3)$$

where ξ is the frequency variable, δ is the Dirac delta function, and $T_1(\xi,b)$ is the quantity transformed from CWT $W_1(a,b)$ on the time-frequency plane [60]. The squeezing and reassigning process is defined as the synchrosqueezed wavelet transform, and $T_1(\xi,b)$ is the synchrosqueezed wavelet coefficient. Through squeezing and reassigning the scale variable of the CWT into a candidate instantaneous frequency variable during the wavelet transform [63], the spectral leakage caused by CWT can be suppressed. Xue et al. [64] compared the performances of the SWT and CWT in monitoring wind turbine blades and found that the SWT can effectively suppress the spectral leakage caused by WT. Hence, the SWT is introduced to replace the CWT in the wavelet transform coherence

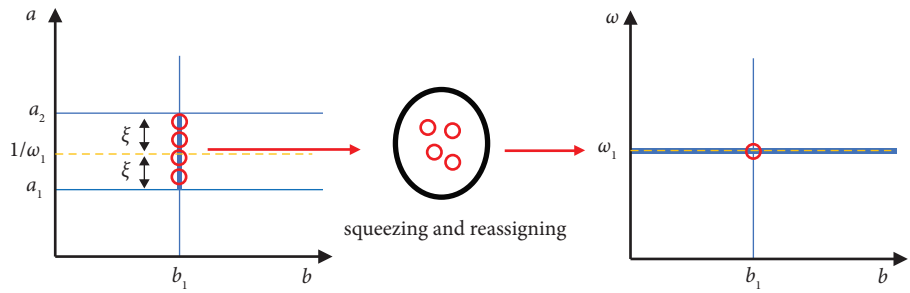

Figure 3: The process of squeezing and reassigning.

recognition method, and the detailed process is described as follows.

Based on the SWT, the autospectrum of the synchrosqueezed wavelet coefficient of the AE signal x_1 can be expressed as follows:

$$T_{1,1}(\eta, b) = T_1(\eta, b) * T_1(\eta, b)^*, \tag{4}$$

where $*$ is the complex conjugate, and the synchrosqueezed wavelet power of the AE signal x_1 is defined as $|T_{1,1}(\eta, b)|$ [55].

The cross-wavelet transform accurately describes the coherency of two signals in the time-frequency domain [65]. Specifically, for the velocity measurement pair $\{x_1, x_2\}$, the cross synchrosqueezed wavelet transform (XSWT) is defined as follows [55]:

$$T_{1,2}(\eta, b) = T_1(\eta, b) * T_2(\eta, b)^*. \tag{5}$$

The synchrosqueezed wavelet power of the XSWT is $|T_{1,2}(\eta, b)|$. Then, the SWTC matrix R_v of the velocity measurement pair can be obtained by normalizing and smoothing $|T_{1,2}(\eta, b)|$ [58]:

$$R_v = \frac{\left|S\left(\eta^{-1} T_{1,2}(\eta, \mathrm{b})\right)\right|}{\left|S\left(\eta^{-1}|T_{1,1}(\eta, b)|\right) \cdot S\left(\eta^{-1}|T_{2,2}(\eta, b)|\right)\right|}, \tag{6}$$

where S is the smoothing function that prevents $R_v = 1$ at all scales and times and η^{-1} is the factor to convert the wavelet power to energy density [65]. The smoothing function S is expressed as follows:

$$S(W) = S_{\text{scale}}\left(S_{\text{time}}(W)\right), \tag{7}$$

where S_{scale} and S_{time} are smoothing operations along the wavelet scale axis and time axis, respectively. The smoothing functions S_{scale} and S_{time} should have a similar footprint as used by the wavelet; therefore, S_{scale} and S_{time} used in the Morlet wavelet are defined as follows [55]:

$$S_{\text{time}}(T(\eta, b))|_\eta = \left(T(\eta, b) * e^{-t_1^2/2\eta^2}\right|_\eta, \tag{8}$$

$$S_{\text{scale}}(T(\eta, b))|_b = (T(\eta, b) * \Pi(\mathrm{cb})), \tag{9}$$

where t_1 denotes the smoothing range. Considering the length of AE signals (1024 signal points), the smoothing range is set to $[-30, 30]$, which can keep a good balance between frequency resolution and significance [55]; c is the scale decorrelation length for the Morlet wavelet, and it is set to 0.6 [54]; Π is the rectangle function. Equations (4)–(9) are similar to the equations of the WTC recognition method [55, 58], but the coefficients T, T_1, and T_2 in the above equations are obtained by the SWT. By suppressing the spectral leakage, the coherence matrix R_v obtained by the SWTC can more accurately characterize the similarity of the velocity measurement pair than the WTC. The improved ability to characterize similarity will be verified by an AE localization experiment described in the Section "Recognition Accuracy of the SWTC Recognition Method."

In order to reduce the influence of subjective factors in observing the coherence graphs, the SWTC coefficient of the coherence matrix R_v is proposed. The element $R_v^{i,j}$ indicates the similarity of the AE signals x_1 and x_2 at the i^{th} line and j^{th} column in the coherence matrix R_v. The line and column of the coherence matrix R_v correspond to the frequency and time, and thus $R_v^{i,j}$ is a gauge for the similarity in the time-frequency domain. Hence, the average value of the coherence matrix R_v^{SWTC} can also reflect the similarity of the velocity measurement pair $\{x_1, x_2\}$ in the time-frequency domain:

$$\frac{c_v = \sum_{i=1}^{M} \sum_{j=1}^{N} R_v^{i,j}(\xi, b)}{M * N}, \tag{10}$$

where M and N are the total numbers of lines and columns of the coherence matrix R_v, respectively. c_v is denoted as the SWTC coefficient of the velocity measurement pair. Similarly, the SWTC coefficient c_l of the localization pair can be obtained in the same way. According to the Schwartz inequality [66], the range of the SWTC matrix is between $[0, 1]$; thus, the range of c_v and c_l are also between $[0, 1]$. In this range, 0 means low coherency and 1 means high coherency, with higher coherency of signals denoting higher similarity.

Therefore, the SWTC coefficients of $\{g_1, g_2, \cdots, g_n\}$ can be expressed as follows:

$$g_l = \left\{c_{l,1}, c_{l,2}, \cdots, c_{l,n}\right\}, \tag{11}$$

$$g_v = \left\{c_{v,1}, c_{v,2}, \cdots, c_{v,n}\right\}. \tag{12}$$

The mean values of g_l and g_v are defined as follows:

$$\text{mean}_l = \text{mean}\{g_l\} = \text{mean}\{c_{l,1}, c_{l,2}, \cdots, c_{l,n}\}, \quad (13)$$

$$\text{mean}_v = \text{mean}\{g_v\} = \text{mean}\{c_{v,1}, c_{v,2}, \cdots, c_{v,n}\}. \quad (14)$$

If a localization group satisfies the following:

$$c_{l,i} \geq \text{mean}_l, \quad (15)$$

$$c_{v,i} \geq \text{mean}_v, \quad (16)$$

the localization group will be regarded as the homologous signal group. Then, the time difference Δt among the homologous signal group is calculated by the SWT picker method [21], and the damage location can be obtained by the following equation:

$$(x_i - x)^2 + (y_i - y)^2 + (z_i - z)^2 = v^2 \Delta t^2, \quad (17)$$

where x, y, and z are each the damage location; x_i, y_i, and z_i are each the sensor location; and v is the wave velocity of the AE signal. Therefore, localization accuracy can be improved by recognizing the localization groups composed of the homologous signals. Furthermore, since the noise is a nonhomologous signal, this recognition process can also filter out the noise.

To sum up, the SWTC recognition method can improve the accuracy in recognizing homologous signals and localization accuracy by suppressing the spectral leakage and quantifying the coherency matrix. In addition, by combining the time-order method, the SWTC recognition method can also improve computational efficiency. An AE localization experiment is used to test the proposed method in the following section.

3. AE Localization Experiment

3.1. Experimental Setup. A steel pipe and a concrete beam served as test specimens. As shown in Figures 4 and 5(a), the inside and the outer diameter of the steel pipe are 78.9 and 88.9 mm, respectively, and the length is 3000 mm. The possible locations of AE sources (the red dots in Figure 4) are assumed to be distributed near the center of the pipe and are separated from each other by 20 mm. The AE signals generated from the AE sources propagate along the steel pipe and are received by the AE sensors (the red rectangles in Figure 4). Five localization distances, including 330 mm, 550 mm, 770 mm, 1210 mm, and 2130 mm, are selected for testing in the experiment.

The size of the concrete beam is 900 × 115 × 80mm, as shown in Figures 5(b) and 6. The strength of the concrete is graded at C60 with its detailed composition listed in Table 1. The locations of manual AE sources (the red dots in Figure 6) are also distributed near the center of the concrete beam and are separated from each other by 20 mm. The possible locations of AE sources (the red dots in Figure 6) are assumed to be distributed along the concrete beam and are separated from each other by 20 mm. Due to the size limitation of the concrete beam, only two localization distances, including 330 mm and 550 mm, are tested in the experiment.

A PCI-2 8-channel AE system (Physical Acoustic Corporation) interrogated four R6a AE sensors (Physical Acoustic Corporation) is shown in Figure 5. The AE sensors have a 35–100 kHz frequency band and a resonance frequency of 55 kHz. Since the approximate range of damage sources can be preliminarily determined, the distributions of sensors are shown in Figure 5, and the detailed information is shown in Figures 4 and 6. According to the authors of [21, 67], the preamplifier is type 2/4/6 (Physical Acoustic Corporation), and its gain and threshold are set to 40 dB and 45 dB, respectively.

As the damage in the specimen grows, the density of collected AE signals gradually increases. However, pencil lead fracture (PLF) [68], a standard method of simulating AE signals, has long interval times and thus only acts on low-density AE signals. To solve this problem, the authors of [21, 69] proposed ball dropping and wrench knocking to simulate the high-density AE signals. In this experiment, PLF is used to simulate low-density AE signals, and wrench knocking (for the steel pipe) and ball dropping (for the concrete beam) are used to simulate high-density AE signals.

The main valuable components of signals are preserved to maintain higher recognition accuracy, while noise components are filtered out. Figure 7 shows the waveform and spectrogram of an AE signal, and it can be found that the energy is concentrated in the 7–70 kHz. Hence, in the frequency domain, the SWTC coefficient and the WTC coefficient are calculated in the range of 7–70 kHz (horizontal red diamond-dashed lines in Figure 7(b)) and thereby avoid noise. In the time domain, the starting point (vertical black triangle-dashed line in Figure 7) is identified by the double-AIC method. The endpoint (vertical orange x-dashed line in Figure 7) corresponds to 0.000556 s. The selection of the area within these points can help minimize the interference of reflected and refracted waves. As illustrated in Figure 7, the computing intervals of the NCC and DTW are between the vertical black triangle-dashed line and orange x-dashed line in Figure 7(a); the computing intervals of the WTC recognition and SWTC recognition methods are the rectangles enclosed by the above four lines in Figure 7(b). For this signal, four methods use the same computing interval of 0.00031 s. In practical engineering, the parameters of computing intervals can be easily obtained from the pre-experiment in the laboratory. Furthermore, the central frequency of the complex Morlet wavelet is 0.955 Hz which can provide a good balance between the time and frequency localization [61].

In the following section, the experimental results are sequentially used to test the recognition accuracy and the localization accuracy of the SWTC recognition method, respectively. The localization error gauges the recognition accuracy of the SWTC recognition method, where a lower localization error denotes higher recognition accuracy. The results of the proposed method are compared with those of three other similarity recognition methods (i.e., the NCC recognition method, the DTW recognition method, and the WTC recognition method). A part of collected AE signals is used to compare the computing time between the traditional recognition methods and the SWTC recognition method.

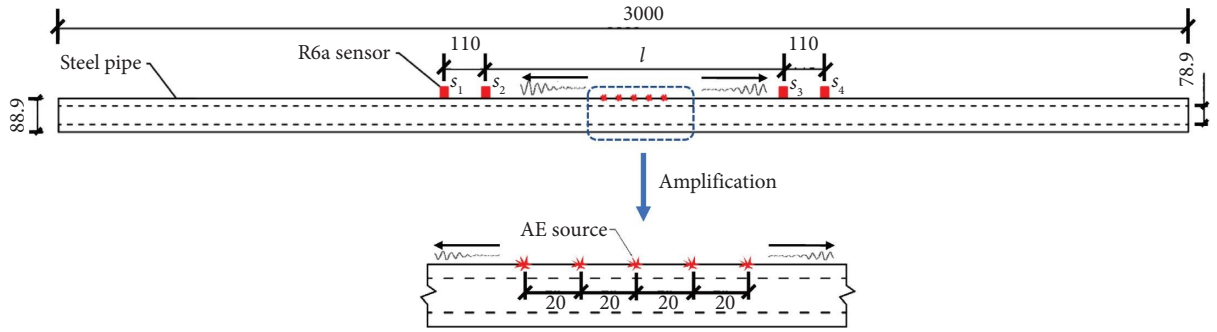

Figure 4: Detailed dimensions of the steel pipe (unit: mm).

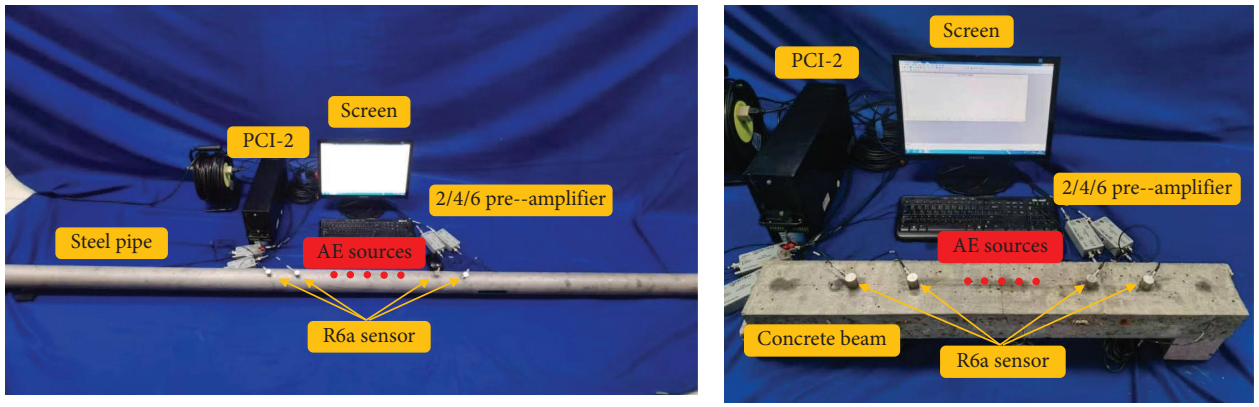

(a) (b)

Figure 5: Photographs of the experiments and the AE devices: (a) steel pipe experiment and (b) concrete beam experiment.

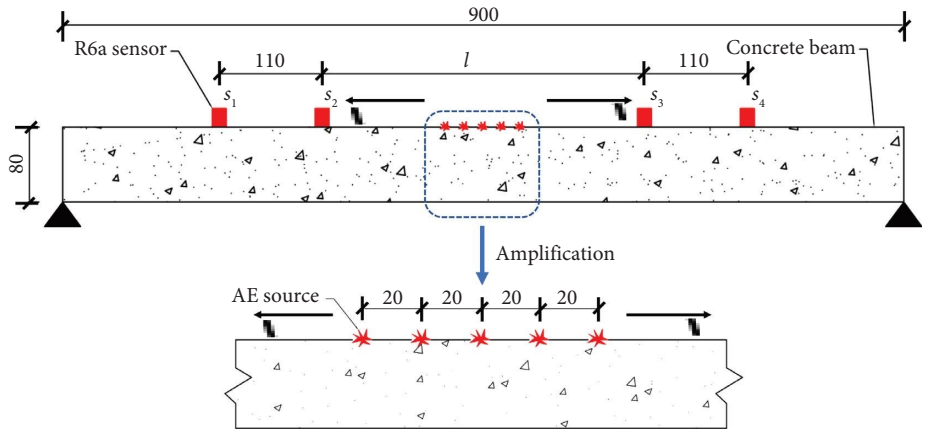

Figure 6: Detailed dimension of the concrete beam (unit: mm).

Table 1: The components of C60 concrete.

Components	Water (%)	Cement (%)	Granite (%)	Sand (%)	Fly ash (%)	Superplasticizer (%)
Rate	5.88	15.83	49.82	25.63	2.48	0.36

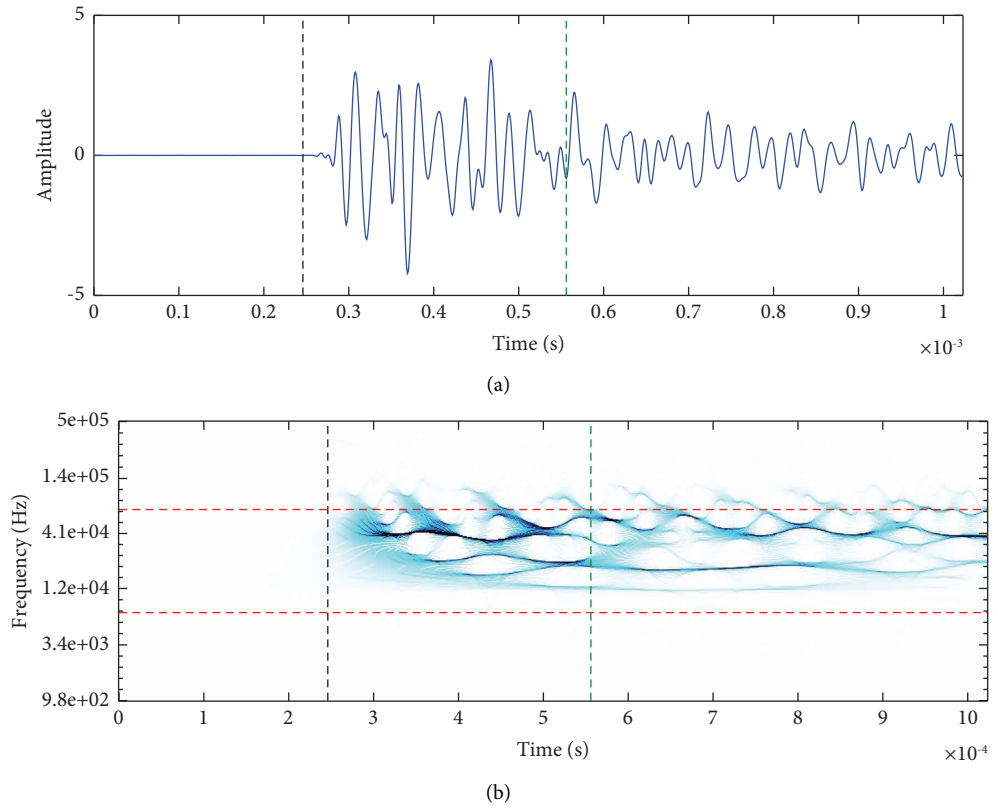

Figure 7: The computing interval of the four recognition methods: (a) time domain and (b) time-frequency domain.

3.2. Recognition Accuracy of the SWTC Recognition Method. For verifying the recognition accuracy of the SWTC recognition method, five testing groups are selected from the above experiment. Each testing group contains 20 pairs of homologous AE signals, which are randomly selected from the sensors s_2 and s_3, as shown in Figures 4 and 6. The 20 pairs of homologous AE signals are divided into two groups:

$$\text{group}_1 = \left\{s_{1,1}, s_{2,1}, \cdots, s_{m,1}\right\}, \tag{18}$$

$$\text{group}_2 = \left\{s_{1,2}, s_{2,2}, \cdots, s_{m,2}\right\}, \tag{19}$$

where $s_{i,1}$ and $s_{i,2}$ are a pair of homologous AE signals, which indicate high similarity, and $m = 20$.

Then, by sequentially computing the similarity values sim_j between the AE signals $s_{j,1}$ from group_1 and all AE signals from group_2, the results can be expressed as follows:

$$\text{sim}_j = \left\{r_{1,j}, r_{2,j}, \cdots, r_{m,j}\right\} = r_{k,j}, \tag{20}$$

where $j = \{1, 2 \cdots m\}$ and $k = \{1, 2 \cdots m\}$. This similarity computing process is called the j^{th} match. If the maximum value $r_{k,j}^{\max}$ of sim_j satisfies $k = j$ in the j^{th} match, the match will be regarded as a successful match. However, when using DTW to calculate the similarity values, it should choose the minimal value $r_{k,j}^{\min}$ of sim_j to check whether the value satisfies $k = j$ in the j^{th} match. The rate of successful matches is

$$\text{rate} = \frac{n}{N}, \tag{21}$$

where n is the number of successful matches and N is the total number of matches. In the following sections, the results of the SWTC recognition method are compared with those of other similarity recognition methods, including the NCC, DTW, and WTC recognition methods.

The results are shown in Figure 8, and the detailed information is listed in Table 2. The NCC and DTW recognition methods have similar successful match rates, which are around 50%. The low successful match rates suggest that the two time domain similarity recognition methods are unsuitable for identifying homologous AE signals. Compared with the NCC and DTW recognition methods, the WTC recognition method has better successful match rates (around 70%) because the WTC recognition method extends the analysis domain from the time domain to the time-frequency domain. The SWTC recognition method further improves the successful math rate to be around 80%.

The observed difference in successful match rates among the WTC and SWTC recognition methods can be attributed to the spectrum leakage, which blurs the time-frequency graph in the WTC recognition method. As shown in Figure 9(a), two AE signals are selected from the above experiment, and the computing intervals of SWTC and WTC coefficients are identical (as shown in Figure 7). The two AE signals are nonhomologous, which means the coherence value between the two signals should be low. Figure 9(b) shows the time-frequency graph transformed by WTC. The figure shows that the

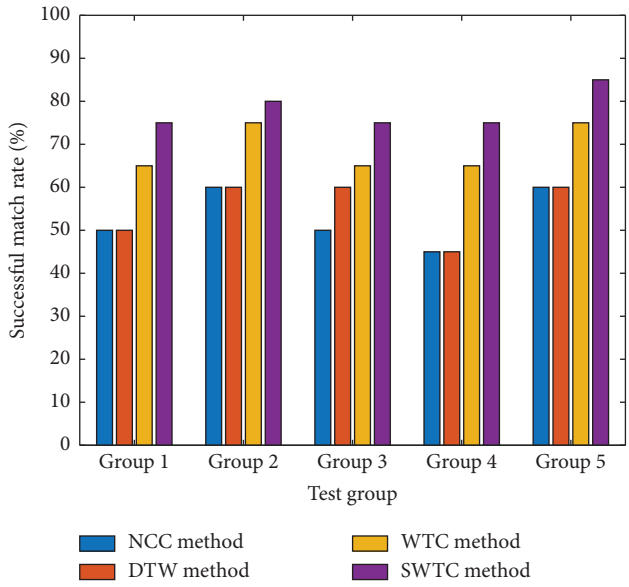

Figure 8: The successful match rates of the five tested groups.

Table 2: The successful match rates of the five tested groups.

Test groups	NCC (%)	DTW (%)	WTC (%)	SWTC (%)
Group 1	50	50	65	75
Group 2	60	60	75	80
Group 3	50	60	65	75
Group 4	45	45	65	75
Group 5	60	60	75	85

spectrum leakage causes the wavelet energy to be vaguely distributed across 10–100 kHz. The vague time-frequency graph further causes the coherency coefficient to diffuse in the coherency graph (as shown in Figure 9(c)), which in turn causes the WTC coefficient of the two AE signals to be high (0.58). Figure 10 shows the results obtained by the SWTC recognition method. Compared with the results of WTC (as shown in Figure 9), the SWTC effectively improves the clarity of the time-frequency graphs by concentrating the wavelet energy to central frequency. Meanwhile, the clear time-frequency graph further enhances the accuracy of the coherence graph (as shown in Figure 10(b)). The SWTC coefficient of the two AE signals is 0.19, which indicates low similarity. Therefore, the SWTC recognition method is demonstrated to have higher accuracy than the WTC recognition method in determining the similarity of AE signals.

The above results verify that the SWTC recognition method yields higher accuracy than other methods in recognizing homologous signals. Hence, the SWTC recognition method should have better localization accuracy than other recognition methods (i.e., the NCC recognition method, DTW recognition method, and WTC recognition method). The localization accuracy will be demonstrated in the following section.

4. Localization Accuracy of the SWTC Recognition Method

4.1. Different Signal Densities. In this section, the above four recognition methods (SWTC recognition method, NCC recognition method, DTW recognition method, and WTC recognition method) are applied to obtain the homologous signals set from the collected signals. Then, the SWT localization method is used to obtain the filtered location values from the homologous signals set. Meanwhile, the unfiltered location values are obtained from the collected signals.

The mean absolute errors (MAE) of the localization values in the low signal density experiments are shown in Figure 11, and the improvement rates (IR) of the localization values are listed in Table 3. The MAE and IR are defined as follows:

$$\mathrm{MAE} = \frac{\sum_{i=1}^{N} \left| l_{\mathrm{mea},i} - l_{\mathrm{true},i} \right|}{N}, \tag{22}$$

$$\mathrm{IR} = \frac{\mathrm{MAE}_{\mathrm{unfiltered}} - \mathrm{MAE}_{\mathrm{filtered}}}{\mathrm{MAE}_{\mathrm{unfiltered}}}, \tag{23}$$

where $l_{\mathrm{mea},i}$ is the calculated localization value; $l_{\mathrm{true},i}$ is the accurate localization value; N is the number of localization values; $\mathrm{MAE}_{\mathrm{unfiltered}}$ is the MAE of unfiltered location values, and $\mathrm{MAE}_{\mathrm{filtered}}$ is the MAE of filtered location values. Through observing equations (22) and (23), it can be found that lower MAE indicates higher localization accuracy and higher IR indicates higher recognition accuracy.

The MAE (31.74 mm) of the DTW recognition method is close to the original MAE (32.21 mm), which causes the IR of the DTW recognition method to be only 1.48%. The NCC recognition method, which operates in the time domain, demonstrated a better performance by improving the MAE and IR to 29.59 mm and 8.13%, respectively. However, the time-frequency similarity recognition methods have higher IR and lower MAE than the time domain similarity recognition methods. The MAE and IR of the WTC recognition method are 17.17 mm and 46.69%, respectively. The SWTC recognition method has the lowest MAE (10.67 mm) and the highest IR (66.86%) out of the four recognition methods, demonstrating that the SWTC has superior recognition accuracy.

The same conclusion can also be obtained from the high signal density experiment (as shown in Figure 11 and Table 3). The SWTC recognition method has the best recognition accuracy by providing the lowest MAE (13.77 mm) and highest IR (56.28%). However, in the SWTC recognition method, the IR (56.28%) of the high signal density experiment is lower than that of the one of the low signal density experiment (66.86%). To assist in understanding this problem, the SWTC recognition method results obtained from the steel pipe experiment and concrete beam experiment are listed in Tables 4 and 5, respectively. The mean amplitudes for low and high signal

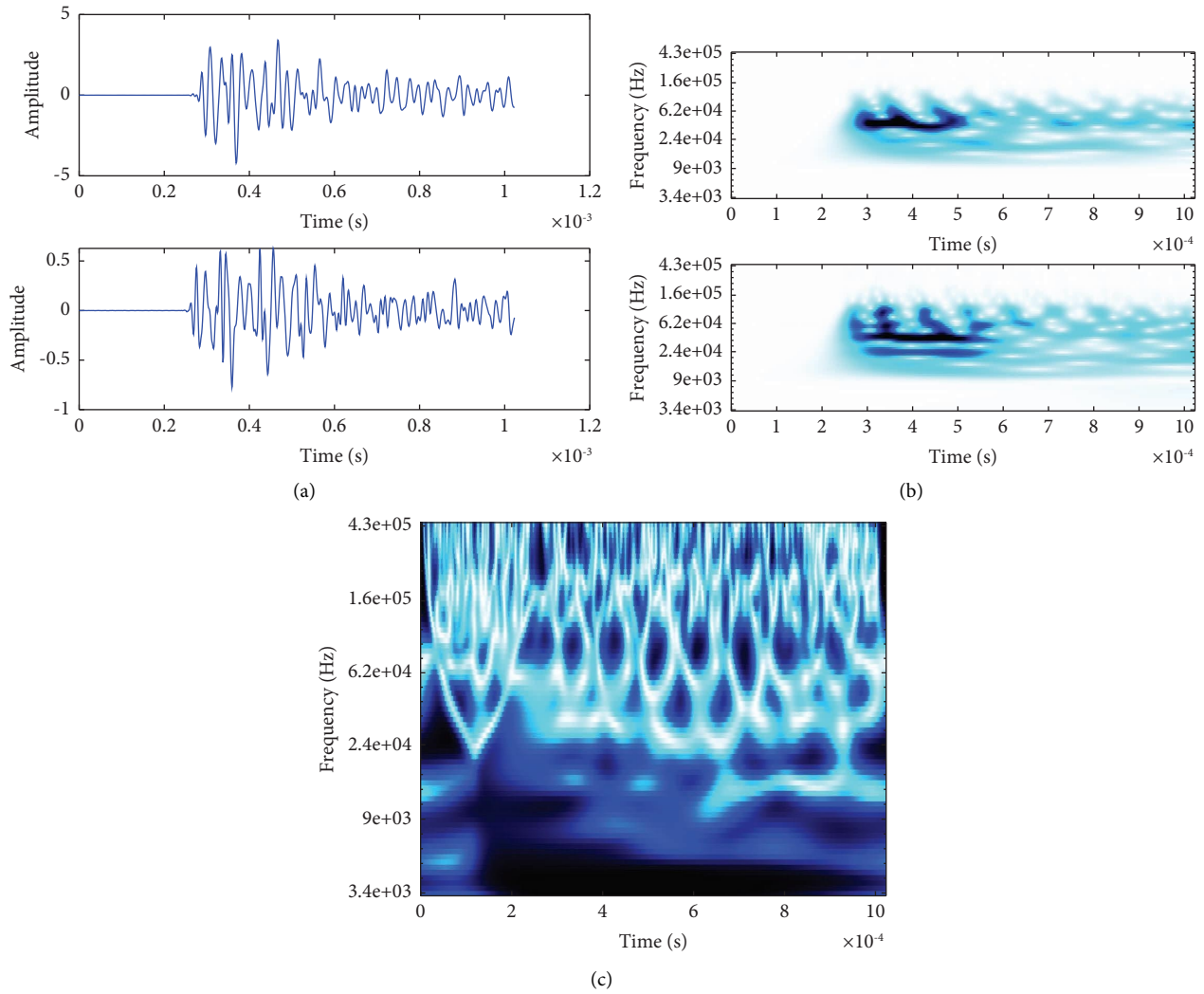

Figure 9: The results of the WTC method: (a) waveforms of two AE signals, (b) WTC time-frequency graphs, and (c) WTC coherency spectrogram.

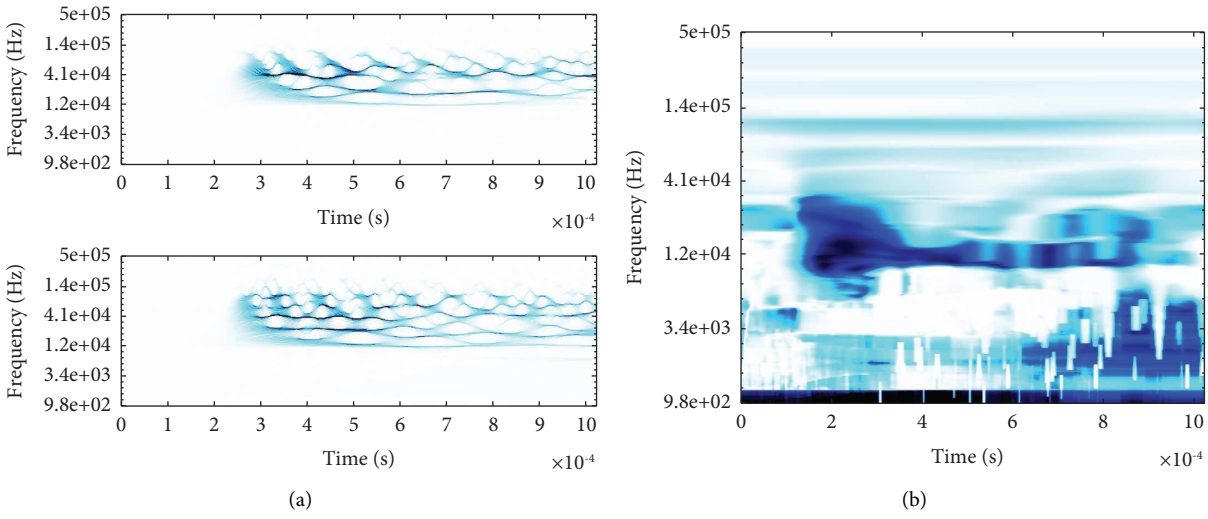

Figure 10: The results of the SWTC method: (a) SWTC time-frequency graphs and (b) SWTC coherency spectrogram.

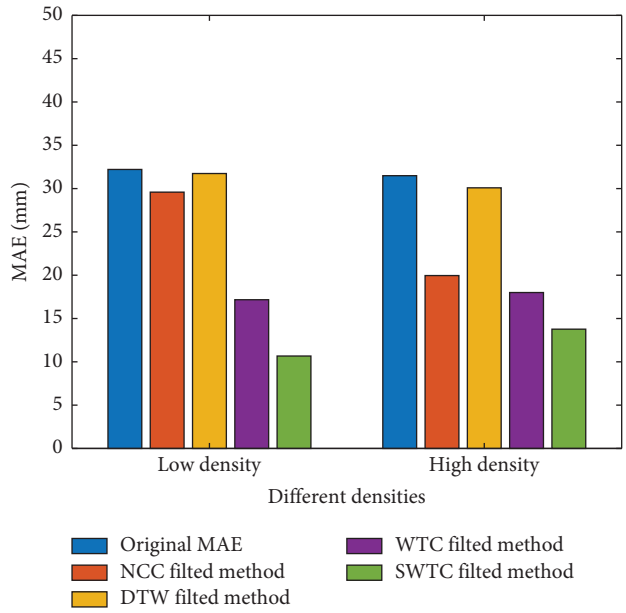

Figure 11: The MAEs of the four recognition methods in different densities.

Table 3: The MAEs and IRs of the four recognition methods for low and high densities.

Densities	MAE (mm)					IR (%)			
	Original	NCC	DTW	WTC	SWTC	NCC	DTW	WTC	SWTC
Low density	32.21	29.59	31.74	17.17	10.67	8.13	1.48	46.69	66.86
High density	31.49	19.96	30.09	18.00	13.77	36.61	4.44	42.82	56.28

Table 4: The MAEs and IRs of different densities in the steel pipe experiment.

Densities	MAE (mm)		IR (%)	Amplitude (dB)
	Original	SWTC	SWTC	
Low density	40.18	12.51	68.87	84.44
High density	38.77	13.16	66.06	83.97

Table 5: The MAEs and IRs of different densities in concrete beam experiment.

Densities	MAE (mm)		IR (%)	Amplitude (dB)
	Original	SWTC	SWTC	
Low density	10.19	5.95	41.63	87.71
High density	20.46	15.10	26.20	77.17

densities in the steel pipe experiment and concrete experiment are also listed in Tables 4 and 5, respectively. The tables show that the mean amplitudes of the steel pipe experiment are similar (around 84 dB) regardless of signal density, and the IRs are also similar (around 67%). In contrast, in the concrete beam experiment, the IR (41.63%) and mean amplitude (87.71 dB) of the low signal density experiment are larger than those of the high signal density experiment (26.2% and 77.17 dB). The lower amplitude of signals means more severe attenuation in transmission, which is not beneficial to the identification of homologous signals. Hence, the problem can be attributed to the low mean amplitudes of the high signal density in the concrete beam experiment. In summary, the SWTC recognition method is better than other recognition methods in improving the localization accuracy across different signal densities by effectively filtering out nonhomologous signals.

4.2. Different Location Distances. Figure 12 shows the MAEs of four recognition methods in different localization distances, and the detailed information is listed in Table 6. Since the concrete beam experiment only has two localization distances (0.33 and 0.55 m), the data in the first two localization distances (0.33 and 0.55 m) contain the results from the steel pipe experiment and the concrete beam experiment. Furthermore, the data in the

Table 6: The MAEs and IRs of the four recognition methods in different localization distances.

Distance (m)	MAE (mm)					IR (%)			
	Original	NCC	DTW	WTC	SWTC	NCC	DTW	WTC	SWTC
0.33	17.90	18.36	16.41	12.99	9.30	−2.53	8.34	27.44	48.06
0.55	24.34	22.32	23.36	14.67	10.65	8.31	4.03	39.71	56.24
0.77	30.73	17.47	28.61	14.16	10.06	43.15	6.91	53.93	67.25
1.21	46.99	32.62	42.06	30.39	19.59	30.58	10.48	35.33	58.31
2.13	49.70	31.28	52.55	28.79	20.55	37.06	−5.74	42.07	58.66

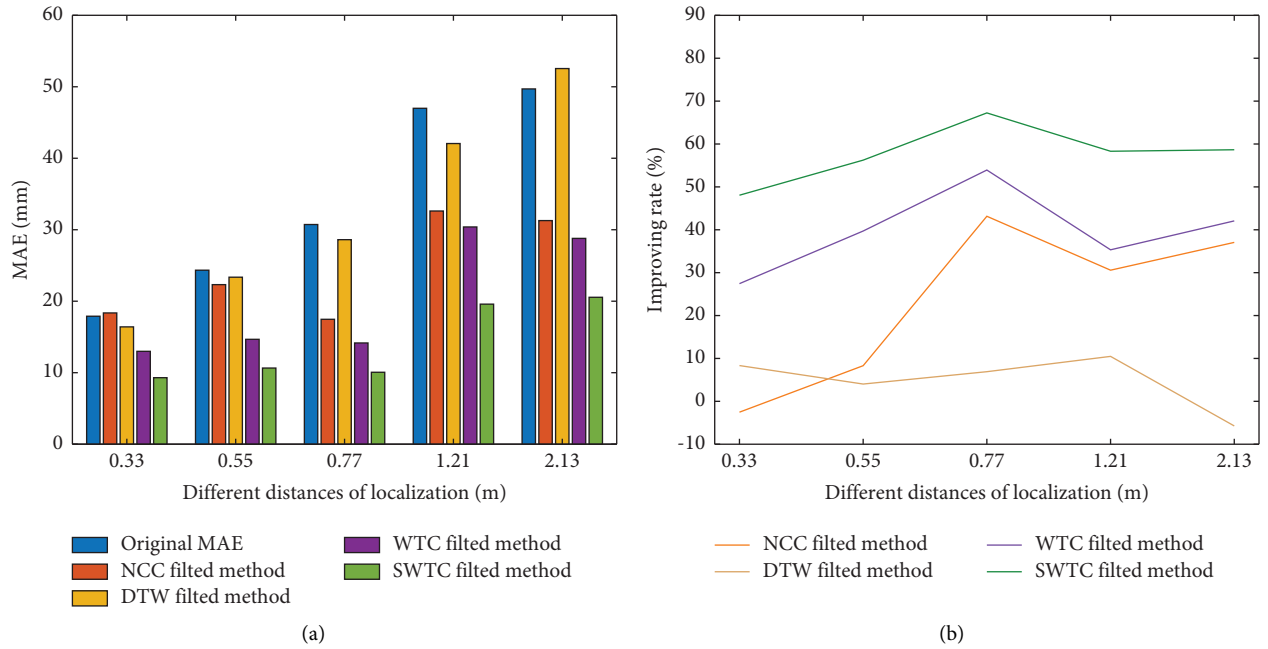

Figure 12: The results of different localization distances: (a) the MAE histogram of the four recognition methods and (b) the IR curves of the four recognition methods.

Table 7: The MAEs and IRs of different localization distances in the steel pipe experiment.

Distance (mm)	MAE (mm)					IR (%)			
	Original	NCC	DTW	WTC	SWTC	NCC	DTW	WTC	SWTC
0.33	16.22	17.36	14.64	8.88	5.83	−7.01	9.79	45.29	60.04
0.55	35.26	30.60	33.98	13.59	8.23	13.20	3.61	61.45	76.65
0.77	30.73	17.47	28.61	14.16	10.06	43.15	6.91	53.93	67.25
1.21	46.99	32.62	42.06	30.39	19.59	30.58	10.48	35.33	58.31
2.13	49.70	31.28	52.55	28.79	20.55	37.06	−5.74	42.07	58.66

later three localization distances (0.77, 1.21, and 2.13 m) only contain the results from the steel pipe experiment.

With the increase in localization distances, the MAEs of the SWTC recognition method are always the lowest among the four recognition methods. The SWTC IR curve, as shown in Figure 12(b), is also almost above 50%. Particularly, in the steel pipe experiment, as shown in Figure 13 and Table 7, the SWTC MAEs reduced significantly in the first two localization distances compared to the results of Table 6, and the IR curve, as shown in Figure 13(b), is almost above 60% in five localization distances. The reason for such performance is discussed in the following section. Compared with other recognition methods, the DTW recognition method has the highest MAEs in the later four localization distances, and the IR curve is below 10% in all localization distances. Particularly at 2.13 m, the IR of the DTW recognition method is negative, which means that the DTW enlarges the localization errors. The same situation also occurred for the NCC recognition method at 0.33 m. These results indicate that the DTW recognition method and NCC recognition method cannot effectively recognize the homologous signals. The above discussion shows that the time-frequency similarity recognition methods outperform the time domain similarity recognition methods in the five localization distances. For the different localization distances, the SWTC recognition

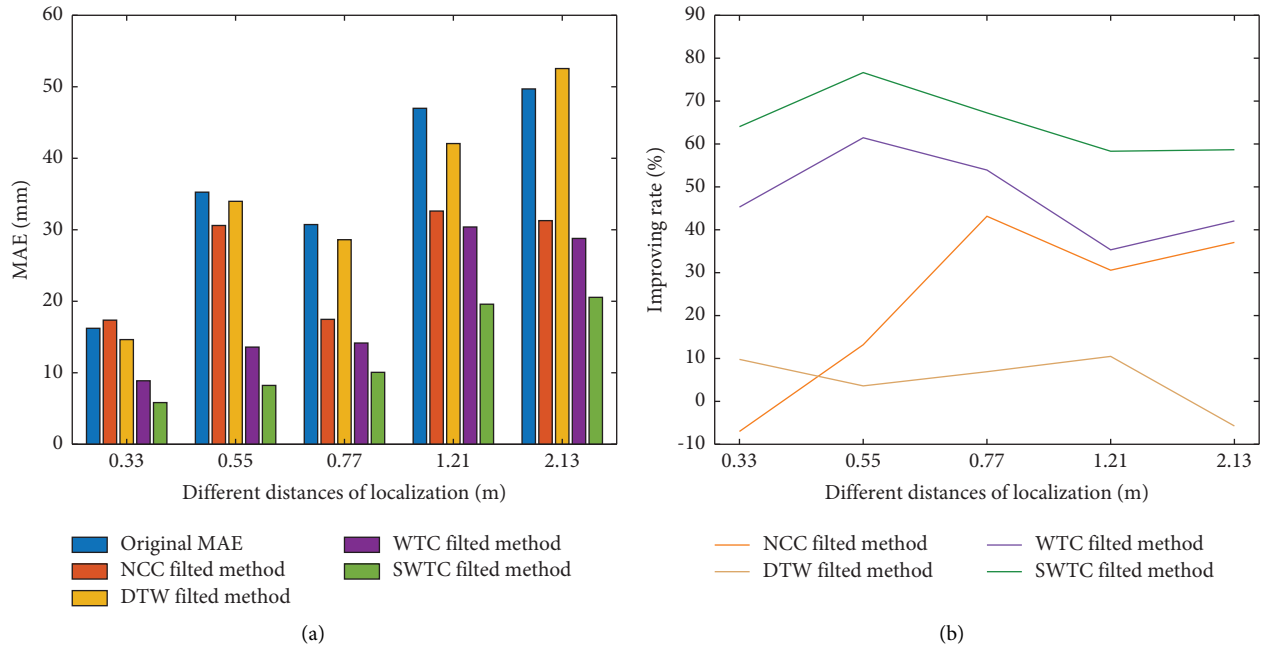

Figure 13: The results of different localization distances in the steel pipe experiment. (a) The MAEs histogram of the four recognition methods and (b) the IRs curves of the four recognition methods.

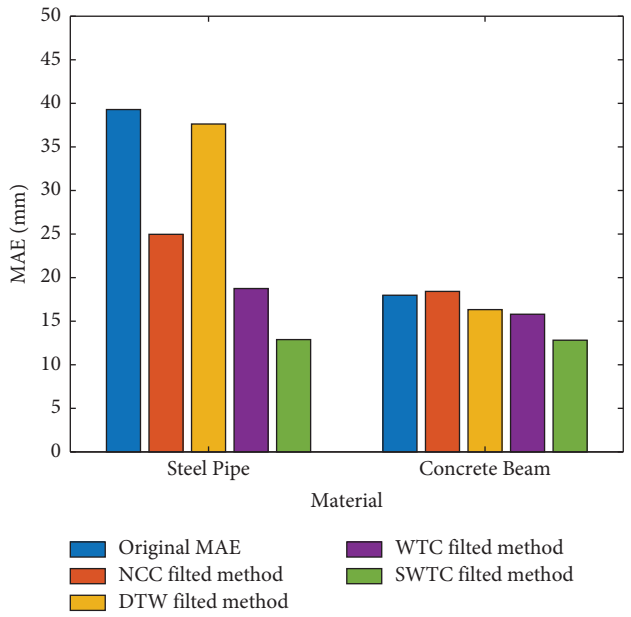

Figure 14: The MAEs of the four recognition methods in the steel pipe and concrete beam.

Table 8: The MAEs and IRs of the four recognition methods in the steel pipe and concrete beam.

Material	MAE (mm)					IR (%)			
	Original	NCC	DTW	WTC	SWTC	NCC	DTW	WTC	SWTC
Steel pipe	39.29	24.97	37.63	18.75	12.89	36.45	4.22	52.29	67.19
Concrete beam	17.98	18.42	16.33	15.8	12.82	−2.42	9.19	12.12	28.68

method effectively reduces localization errors by filtering out the nonhomologous signals, thus indicating the method can accurately identify homologous signals.

4.3. Different Materials. The experimental results from the steel pipe and concrete beam are shown in Figure 14, and the detailed information is listed in Table 8. Compared with other recognition methods, the SWTC recognition method has demonstrated its superior recognition accuracy by providing the lowest MAEs and highest IRs in the two tested material specimens. However, the IR of the SWTC recognition method in the steel pipe experiment is larger than that in the concrete beam experiment, and the same situation also occurred for the NCC and WTC recognition methods. The reason can be attributed to the inhomogeneity of concrete. Inhomogeneity in the material can cause severe frequency dispersion and severe attenuation when the stress wave propagates through the material. The dispersion and attenuation can unpredictably modulate the energy distribution in the time-frequency matrix and cause the coherent matrix to be inaccurate. The IRs of the DTW recognition method are below 10% in both the steel pipe and concrete beam, which means that this method cannot accurately identify the homologous signals. In summary, the SWTC recognition method effectively improves the localization accuracy by filtering out the nonhomologous signals for both tested materials, including one that is inhomogeneous.

5. Discussion

The analysis of the above results shows that the DTW and NCC recognition methods have high MAEs and low IRs, and they fail to identify the homologous signals accurately and cannot improve the localization accuracy. The WTC recognition method offered improved recognition than the above two recognition methods. However, the proposed SWTC recognition method has the lowest MAEs and highest IRs regardless of signal density, location distance, and material. Thus, this method has the best recognition accuracy of homologous signals and localization accuracy among the four tested recognition methods. The conclusion of the section is consistent with the Section "Recognition Accuracy of the SWTC Recognition Method."

To verify the computational efficiency of the proposed SWTC recognition method, 40 AE signals are randomly selected from the above AE localization experiment. The computer CPU is an Intel Core i5-6402P, and the computing software is Matlab R2018a (MathWorks). The computing time taken by the traditional algorithm is 515.74 s, and that of the SWTC recognition method is only 10.19 s. Therefore, the SWTC recognition method effectively reduces the computing time.

6. Conclusion

In this study, a novel SWTC recognition method is proposed to improve the recognition accuracy of homologous AE signals. The spectral analysis of AE signals shows that the proposed recognition method can obtain the explicit coherence graph of AE signals by effectively suppressing the spectral leakage in the time-frequency graph. Then, the SWTC coefficient obtained from the explicit coherence graph can reduce the influence of subjective factors. Two AE localization experiments were implemented on a steel pipe and a concrete beam to test the proposed recognition method. The results demonstrate that the SWTC recognition method has the best recognition accuracy among the four tested recognition methods and further improves the AE localization accuracy across different materials, signal densities, and localization distances by filtering out nonhomologous signals. In particular, for the steel pipe experiment, the improving rate offered by the SWTC recognition method is above 60%, which is much higher than that of the other recognition methods. Hence, the SWTC recognition method can improve localization accuracy by accurately filtering out the nonhomologous AE signals.

However, the proposed method also has some limitations. The selection of the frequency bands for filtering and calculation range requires prior information about the structure and its boundary conditions; the damage size and shape could not be identified. In future research, there are plans to combine the clustering technique and active detection technique with the SWTC recognition method. This integration aims to automatically search for the appropriate calculation range in the scalogram and assess the shape of the damage. To validate the effectiveness of the proposed method, extensive experiments will be conducted on large-scale specimens. Furthermore, the accurate damage source and AE parameters will be used to convert the time-frequency domain to the wavenumber-frequency domain, which can show more information about the damage. The types and degree of damage will be easily identified in the wavenumber-frequency domain.

Data Availability

The data used to support the findings of this study are available from the corresponding author upon request.

Conflicts of Interest

The authors declare that there are no conflicts of interest.

Acknowledgments

This work was partially supported by the National Natural Science Foundation of China (grant number 52178274) and the Dalian High Level Talent Innovation Support Program (grant number 2019RD01). The authors would like to thank for these financial supports. Some of the synchrosqueezed wavelet transforms (SWT) signal processing programs in this paper were based on those by Eugene Brevdo (https://www.math.princeton.edu/~ebrevdo/).

References

[1] D. Li, M. Tan, S. Zhang, and J. Ou, "Stress corrosion damage evolution analysis and mechanism identification for

prestressed steel strands using acoustic emission technique," *Structural Control and Health Monitoring*, vol. 25, no. 8, p. 2189, 2018.

[2] N. Li, F. Wang, and G. Song, "New entropy-based vibro-acoustic modulation method for metal fatigue crack detection: an exploratory study," *Measurement*, vol. 150, Article ID 107075, 2020.

[3] A. Gheitasi and D. K. Harris, "Overload flexural distribution behavior of composite steel girder bridges," *Journal of Bridge Engineering*, vol. 20, no. 5, Article ID 4014076, 2015.

[4] J. Jiao, J. Guo, K. Fujita, and I. Takewaki, "Displacement measurement and nonlinear structural system identification: a vision-based approach with camera motion correction using planar structures," *Structural Control and Health Monitoring*, vol. 28, no. 8, 2021.

[5] F. Wang, Z. Chen, and G. Song, "Monitoring of multi-bolt connection looseness using entropy-based active sensing and genetic algorithm-based least square support vector machine," *Mechanical Systems and Signal Processing*, vol. 136, Article ID 106507, 2020.

[6] S. Mahato, M. V. Teja, and A. Chakraborty, "Combined wavelet-Hilbert transform-based modal identification of road bridge using vehicular excitation," *Journal of Civil Structural Health Monitoring*, vol. 7, no. 1, pp. 29–44, 2017.

[7] T. Bao and Z. Liu, "Vibration-based bridge scour detection: a review," *Structural Control and Health Monitoring*, vol. 24, no. 7, p. 1937, 2017.

[8] C. Chen, X. Chen, W. Xu, and X. Cheng, "Fracture behavior and crack mode of steel slag pervious concrete using acoustic emission technique," *Structural Control and Health Monitoring*, vol. 28, no. 9, p. 2796, 2021.

[9] A. Carpinteri, G. Lacidogna, and G. Niccolini, "Damage analysis of reinforced concrete buildings by the acoustic emission technique," *Structural Control and Health Monitoring*, vol. 18, no. 6, pp. 660–673, 2011.

[10] S. De Santis and A. K. Tomor, "Laboratory and field studies on the use of acoustic emission for masonry bridges," *NDT & E International*, vol. 55, pp. 64–74, 2013.

[11] T. Jiang, Q. Kong, D. Patil, Z. Luo, L. Huo, and G. Song, "Detection of debonding between fiber reinforced polymer bar and concrete structure using piezoceramic transducers and wavelet packet analysis," *IEEE Sensors Journal*, vol. 17, no. 7, pp. 1992–1998, 2017.

[12] A. Maslouhi, "Fatigue crack growth monitoring in aluminum using acoustic emission and acousto-ultrasonic methods," *Structural Control and Health Monitoring*, vol. 18, no. 7, pp. 790–806, 2011.

[13] R. Guan, Y. Lu, W. Duan, and X. Wang, "Guided waves for damage identification in pipeline structures: a review," *Structural Control and Health Monitoring*, vol. 24, no. 11, p. 2007, 2017.

[14] S. Liu, C. Wu, J. Zhou et al., "Relation between the shear stress distribution and the resulting acoustic emission variation in concrete beams," *Structural Control and Health Monitoring*, vol. 27, no. 6, 2020.

[15] A. Carpinteri, A. Grazzini, G. Lacidogna, and A. Manuello, "Durability evaluation of reinforced masonry by fatigue tests and acoustic emission technique," *Structural Control and Health Monitoring*, vol. 21, no. 6, pp. 950–961, 2014.

[16] F. Q. Su, K. Itakura, G. Deguchi, and K. Ohga, "Monitoring of coal fracturing in underground coal gasification by acoustic emission techniques," *Applied Energy*, vol. 189, pp. 142–156, 2017.

[17] C. Giannì, M. Balsi, S. Esposito, and F. Ciampa, "Low-power global navigation satellite system-enabled wireless sensor network for acoustic emission localisation in aerospace components," *Structural Control and Health Monitoring*, vol. 27, no. 6, 2020.

[18] J. Xu, Z. Fu, Q. Han, and H. Li, "Fracture monitoring and damage pattern recognition for carbon nanotube-crumb rubber mortar using acoustic emission techniques," *Structural Control and Health Monitoring*, vol. 26, no. 10, 2019.

[19] M. Kaphle, A. C. C. Tan, D. P. Thambiratnam, and T. H. T. Chan, "Identification of acoustic emission wave modes for accurate source location in plate-like structures," *Structural Control and Health Monitoring*, vol. 19, no. 2, pp. 187–198, 2012.

[20] S. Li, Z. Liu, L. Xia, Y. Wang, and H. Feng, "Wire breaking localization of parallel steel wire bundle using acoustic emission tests and finite element analysis," *Structural Control and Health Monitoring*, vol. 28, no. 3, 2021.

[21] J. Wang, L. Huo, C. Liu, and G. Song, "A new acoustic emission damage localization method using synchrosqueezed wavelet transforms picker and time-order method," *Structural Health Monitoring*, vol. 20, no. 6, pp. 2917–2935, 2020.

[22] S. Chen, C. Yang, G. Wang, and W. Liu, "Similarity assessment of acoustic emission signals and its application in source localization," *Ultrasonics*, vol. 75, pp. 36–45, 2017.

[23] T. Warren Liao, "Clustering of time series data- a survey," *Pattern Recognition*, vol. 38, no. 11, pp. 1857–1874, 2005.

[24] M. Vlachos, K. George, and D. Gunopulos, "Discovering similar multidimensional trajectories," in *Proceedings of the 18th International Conference on Data Engineering*, pp. 673–684, San Jose, CA, USA, February 2002.

[25] P. K. Chan and M. V. Mahoney, "Modeling multiple time series for anomaly detection," in *Proceedings of the 5th IEEE International Conference on Data Mining*, p. 8, Houston, Texas, November 2006.

[26] Z. Lv, B. Zhang, X. Wu, C. Zhang, and B. Zhou, "A permutation algorithm based on dynamic time warping in speech frequency-domain blind source separation," *Speech Communication*, vol. 92, pp. 132–141, 2017.

[27] J. Chen and X. Xu, "Android voiceprint unlocking system based on Mel frequency cepstrum coefficient and dynamic time warping," *Computer Engineering*, vol. 43, no. 2, pp. 201–205, 2017.

[28] Y. S. Jeong, M. K. Jeong, and O. A. Omitaomu, "Weighted dynamic time warping for time series classification," *Pattern Recognition*, vol. 44, no. 9, pp. 2231–2240, 2011.

[29] K. Yu, G. D. Guo, J. Li, and S. Lin, "Quantum algorithms for similarity measurement based on euclidean distance," *International Journal of Theoretical Physics*, vol. 59, no. 10, pp. 3134–3144, 2020.

[30] Z. Zheng, Y. Li, S. He, X. Ma, X. Zhu, and S. Li, "High density and high strength cement-based mortar by modification with epoxy resin emulsion," *Construction and Building Materials*, vol. 197, pp. 319–330, 2019.

[31] H. Izakian, W. Pedrycz, and I. Jamal, "Fuzzy clustering of time series data using dynamic time warping distance," *Engineering Applications of Artificial Intelligence*, vol. 39, pp. 235–244, 2015.

[32] H. Sakoe and S. Chiba, "A dynamic programming approach to continuous speech recognition," in *Proceedings of the 7th International Congress on Acoustics*, pp. 65–68, Budapes, Europe, September 1971.

[33] S. K. Sharma, H. Phan, and J. Lee, "An application study on road surface monitoring using DTW based image processing

and ultrasonic sensors," *Applied Sciences*, vol. 10, no. 13, p. 4490, 2020.

[34] H. M. El-Bakry and Q. Zhao, "Fast pattern detection using normalized neural networks and cross-correlation in the frequency domain," *EURASIP Journal on Advances in Signal Processing*, vol. 2005, no. 13, pp. 404897–412060, 2005.

[35] M. I. Vakil, J. A. Malas, and D. B. Megherbi, "An information theoretic metric for identifying optimum solution for normalized cross correlation based similarity measures," in *Proceedings of the 2015 IEEE National Aerospace and Electronics Conference*, pp. 136–140, Dayton, Ohio, June 2015.

[36] C. Chiu, T. Lin, and B. Y. Liau, "Using correlation coefficient in ECG waveform for arrhythmia detection," *Biomedical Engineering: Applications, Basis and Communications*, vol. 17, no. 3, pp. 147–152, 2005.

[37] R. M. Aarts, R. M. Irwan, and A. Janssen, "Efficient tracking of the cross-correlation coefficient," *IEEE Transactions on Speech and Audio Processing*, vol. 10, no. 6, pp. 391–402, 2002.

[38] G. Jacovitti and R. Cusani, "An efficient technique for high correlation estimation," *IEEE Transactions on Acoustics, Speech, & Signal Processing*, vol. 35, no. 5, pp. 654–660, 1987.

[39] M. C. Andreea and M. Gabrea, "Correlation coefficient-based voice activity detector algorithm," in *Proceedings of the Canadian Conference on Electrical and Computer Engineering 2004*, pp. 1789–1792, Niagara Falls, North America, May 2004.

[40] M. Hilbrich and R. Muller-Pfefferkorn, "Cross-correlation as tool to determine the similarity of series of measurements for big-data analysis tasks," in *Proceedings of the Cloud Computing and Big Data. Second International Conference, CloudCom-Asia 2015*, pp. 263–282, Huangshan, China, January 2015.

[41] A. Klausen and K. G. Robbersmyr, "Cross-correlation of whitened vibration signals for low-speed bearing diagnostics," *Mechanical Systems and Signal Processing*, vol. 118, pp. 226–244, 2019.

[42] L. T. Nguyen, G. K. Kocur, and E. H. Saenger, "Defect mapping in pipes by ultrasonic wavefield cross-correlation: a synthetic verification," *Ultrasonics*, vol. 90, pp. 153–165, 2018.

[43] L. Zhao, J. Wang, M. Hou, and Z. Li, "Negative pressure wave leakage location algorithm based on difference cross-correlation delay estimation," *IOP Conference Series: Materials Science and Engineering*, IOP Publishing Ltd, vol. 612, no. 4, p. 42047, Yunnan, China, 2019.

[44] J. Xi, B. Xiao, H. Ma, and Q. Wang, "Research on acoustic emission source location method based on cross-correlation analysis without measuring sonic speed," in *Proceedings of the 26th Chinese Control and Decision Conference*, pp. 4392–4395, Changsha, China, May 2014.

[45] T. Permana, T. Nishimura, H. Nakahara, E. Fujita, and H. Ueda, "Reliability evaluation of volcanic tremor source location determination using cross-correlation functions," *Geophysical Journal International*, vol. 220, no. 2, pp. 1300–1315, 2020.

[46] A. Johannes, H.-P. Kriegel, K. Pal, K. Pascal, A. S. Pryakhin, and M. P. Renz, "Similarity search on time series based on threshold queries," in *Proceedings of the 10th International Conference on Extending Database Technology Munich*, pp. 276–294, Berlin, Heidelberg, June 2006.

[47] L. Stankovic, I. Djurovic, S. Stanković, M. Simeunovic, S. Djukanovic, and M. Dakovic, "Instantaneous frequency in time-frequency analysis: Enhanced concepts and performance of estimation algorithms," *Digital Signal Processing*, vol. 35, pp. 1–13, 2014.

[48] Y. Yang, Z. Peng, W. Zhang, and G. Meng, "Parameterised time-frequency analysis methods and their engineering applications: a review of recent advances," *Mechanical Systems and Signal Processing*, vol. 119, pp. 182–221, 2019.

[49] A. Katunin, "Vibration-based spatial damage identification in honeycomb-core sandwich composite structures using wavelet analysis," *Composite Structures*, vol. 118, pp. 385–391, 2014.

[50] G. Sun, Y. Wang, Q. Luo, and Q. Li, "Vibration-based damage identification in composite plates using 3D-DIC and wavelet analysis," *Mechanical Systems and Signal Processing*, vol. 173, Article ID 108890, 2022.

[51] A. Chakraborty, B. Basu, and M. Mitra, "Identification of modal parameters of a mdof system by modified L-P wavelet packets," *Journal of Sound and Vibration*, vol. 295, no. 3-5, pp. 827–837, 2006.

[52] B. Basu, S. Nagarajaiah, and A. Chakraborty, "Online identification of linear time-varying stiffness of structural systems by wavelet analysis," *Structural Health Monitoring*, vol. 7, no. 1, pp. 21–36, 2008.

[53] S. Mahato and A. Chakraborty, "Sequential clustering of synchrosqueezed wavelet transform coefficients for efficient modal identification," *Journal of Civil Structural Health Monitoring*, vol. 9, no. 2, pp. 271–291, 2019.

[54] C. E. Torrence and G. P. Compo, "A practical guide to wavelet analysis," *Bulletin of the American Meteorological Society*, vol. 79, no. 1, pp. 61–78, 1998.

[55] Z. Gao, J. Lin, X. Wang, and Y. Liao, "Grinding burn detection based on cross wavelet and wavelet coherence analysis by acoustic emission signal," *Chinese Journal of Mechanical Engineering*, vol. 32, no. 1, p. 68, 2019.

[56] A. Grinsted, J. C. Moore, and S. Jevrejeva, "Application of the cross wavelet transform and wavelet coherence to geophysical time series," *Nonlinear Processes in Geophysics*, vol. 11, no. 5/6, pp. 561–566, 2004.

[57] G. Kramer, A. Van der Stouwe, N. M. Maurits, M. A. J. Tijssen, and J. W. J. Elting, "Wavelet coherence analysis: a new approach to distinguish organic and functional tremor types," *Clinical Neurophysiology*, vol. 129, no. 1, pp. 13–20, 2018.

[58] C. E. Torrence and P. J. Webster, "Interdecadal changes in the ENSO-monsoon system," *Journal of Climate*, vol. 12, no. 8, pp. 2679–2690, 1999.

[59] C. Li and M. Liang, "A generalized synchrosqueezing transform for enhancing signal time-frequency representation," *Signal Processing*, vol. 92, no. 9, pp. 2264–2274, 2012.

[60] Q. Jiang and B. W. Suter, "Instantaneous frequency estimation based on synchrosqueezing wavelet transform," *Signal Processing*, vol. 138, pp. 167–181, 2017.

[61] X. Zhang, Y. He, R. Hao, and F. Chu, "Parameters optimization of continuous wavelet transform and its application in acoustic emission signal analysis of rolling bearing," *Chin J Mech Eng-En*, vol. 20, no. 2, pp. 108–112, 2007.

[62] I. Daubechies, J. Lu, and H. T. Wu, "Synchrosqueezed wavelet transforms: an empirical mode decomposition-like tool," *Applied and Computational Harmonic Analysis*, vol. 30, no. 2, pp. 243–261, 2011.

[63] Z. Liu, K. Xu, D. Li, D. Ta, and W. Wang, "Automatic mode extraction of ultrasonic guided waves using synchrosqueezed wavelet transform," *Ultrasonics*, vol. 99, Article ID 105948, 2019.

[64] X. Xue, D. Sun, L. Gu, and Q. Wang, "Application of synchrosqueezed wavelet transforms in Lamb wave based structural health monitoring of wind turbine blades," in

Proceedings of the 31st Chinese Control And Decision Conference, pp. 3190–3195, Nanchang, China, June 2019.

[65] S. Firouzi and X. Wang, "A comparative study of exchange rates and order flow based on wavelet transform coherence and cross wavelet transform," *Economic Modelling*, vol. 82, pp. 42–56, 2019.

[66] Z. Zhang, L. Yue, Y. Yang, X. Xiao, and S. Ge, "Comparative study on wavelet coherence and HHT coherence," in *Proceedings of the 7th International Congress on Image and Signal Processing*, pp. 867–872, Dalian, China, October 2014.

[67] J. Wang, L. Huo, C. Liu, and G. Song, "Wear degree quantification of pin connections using parameter-based analyses of acoustic emissions," *Sensors*, vol. 18, no. 10, p. 3503, 2018.

[68] M. N. Noorsuhada, "An overview on fatigue damage assessment of reinforced concrete structures with the aid of acoustic emission technique," *Construction and Building Materials*, vol. 112, pp. 424–439, 2016.

[69] A. K. Das and C. K. Y. Leung, "A new power-based method to determine the first arrival information of an acoustic emission wave," *Structural Health Monitoring*, vol. 18, no. 5-6, pp. 1620–1632, 2019.